Chemical Science

EDGE ARTICLE

View Article Online
View Journal | View Issue

Cite this: *Chem. Sci.*, 2018, **9**, 2774

Two-photon fluorescent polysiloxane-based films with thermally responsive self switching properties achieved by a unique reversible spirocyclization mechanism†

Yujing Zuo, Tingxin Yang, Yu Zhang, Zhiming Gou, Minggang Tian, Xiuqi Kong and Weiying Lin*

Responsiveness and reversibility are present in nature, and are ubiquitous in biological systems. The realization of reversibility and responsiveness is of great importance in the development of properties and the design of new materials. However, two-photon fluorescent thermal-responsive materials have not been reported to date. Herein, we engineered thermally responsive polysiloxane materials (**Dns-non**) that exhibited unique two-photon luminescence, and this is the first report about thermally responsive luminescent materials with two-photon fluorescence. The fluorescence of **Dns-non** could switch from the "on" to "off" state through a facile heating and cooling process, which could be observed by the naked eye. Monitoring the temperature of the CPU *in situ* was achieved by easily coating **D1-non** onto the CPU surface, which verified the potential application in devices of **Dns-non**. A unique alkaline tuned reversible transition mechanism of rhodamine-B from its spirocyclic to its ring-open state was proposed. Furthermore, **Dns-non** appeared to be a useful cell adhesive for the culture of cells on the surface. We believe that the constructed thermally responsive silicon films which have promising utilization as a new type of functional fluorescent material, may show broad applications in materials chemistry or bioscience.

Received 28th November 2017
Accepted 5th February 2018

DOI: 10.1039/c7sc05080a

rsc.li/chemical-science

Introduction

Responsiveness and reversibility are present in nature, and are ubiquitous in biological systems. In the past decade, the realization of reversibility and responsiveness has been of great importance in the development of properties and the design of new materials.[1–3] Fluorescent responsive systems have received more attention for their facile signal detection method, and for the availability of a large number of examples such as sensors or probes.[4] Besides this, temperature is an important environmental property, therefore, the development of fluorescence-based thermo-sensitive materials is desirable since such a sensor is effective in monitoring temperature *via* detecting fluorescence signals.[5–8] Previously reported fluorescent temperature responsive systems have been mainly based on twisted intramolecular charge-transfer (TICT) fluorophores,[9] cyclodextrin-based phosphorescent compounds,[10] spin crossover complexes,[11] quantum dots,[12] quasi-reversible photodissociation,[13] and lanthanide complexes.[14] However, these fluorescent thermally responsive materials could only emit single photon fluorescence. Two-photon fluorescence has been applied in luminescent imaging techniques due to its unique advantages, including low photodamage to the samples, weak background fluorescence, and high spatial resolution.[15–22] To the best of our knowledge, two-photon fluorescent thermally responsive materials have not been reported to date. Taking into account the merits of both thermally responsive materials and two-photon fluorescence, construction of two-photon fluorescent thermally responsive systems is of great interest and importance. However, there are two vital challenges remaining for designing these systems. First, most reports on thermo-responsive polymers are based on traditional temperature responsive groups such as *N*-isopropylacrylamides, which are non-fluorescent. In addition, traditional functional fluorophores with two-photon absorption do not show thermally responsive properties. Our initial intention here was to build a thermally responsive system with unique two-photon fluorescence; thus, we envisaged the possibility of exploiting a novel responding mechanism realized by the interactions between the functional groups within the polymer base and the fluorescent dye.

Considering that tertiary amines show alkaline properties and have a tendency to react with acid to form a salt, we selected benzoxazine-containing polysiloxanes (**P1**) which contained the tertiary amine as a key structural element. Furthermore, as

Institute of Fluorescent Probes for Biological Imaging, School of Chemistry and Chemical Engineering, School of Materials Science and Engineering, University of Jinan, Shandong 250022, P. R. China. E-mail: weiyinglin2013@163.com

† Electronic supplementary information (ESI) available. See DOI: 10.1039/c7sc05080a

a two-photon fluorescent dye, rhodamine-B based fluorescent probes could act as "turn-on" fluorescent switch molecules in response to the targeted cation.[23–25] The ion detection mechanism of rhodamine probes is mainly based on the change in structure between its open-cycle and spirocyclic states; thus, we anticipated that the presence of its five-membered ring "opening or closing" states could be critical for thermally responsive properties. Then, we intended to incorporate rhodamine-B into **P1** to investigate the novel luminescent responsive properties. Furthermore, rhodamine-B was chosen as the fluorescent moiety, not only for its luminescent performance but, more importantly, for the larger abundance of benzene structures that could make it possible to render physical cross-linking sites on the polysiloxane base.

Herein, rhodamine-B was incorporated into **P1**, which acted both as a physical cross-linker and luminophore. Transparent films of **Dns-non** were obtained and they emitted strong photoluminescence under natural light or UV irradiation. Two-photon luminescence of **Dns-non** was detected. More interestingly, the fluorescence intensity of **Dns-non** exhibited thermally responsive properties, which could be observed by the naked eye. Furthermore, **Dns-non** were applied in devices by monitoring the CPU surface temperature *in situ*. In addition, HeLa cells were cultured on the surfaces of **Dns-non** to investigate their cytocompatibility and to explore their potential applications in biomedical fields.

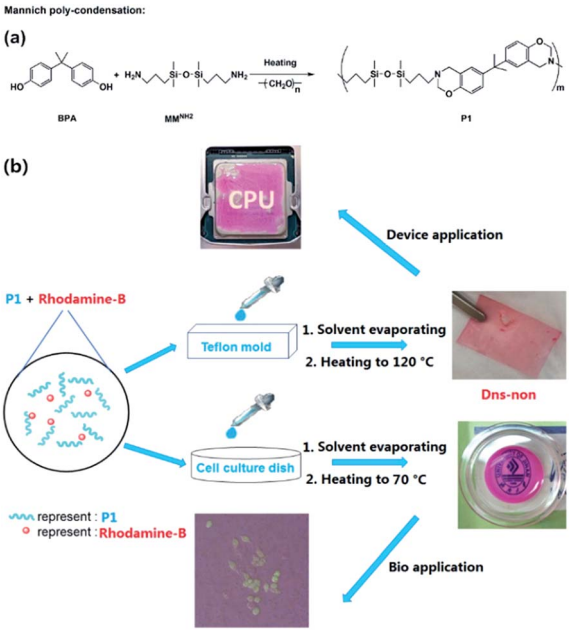

Scheme 1 (a) Synthesis of **P1** by Mannich polycondensation, and (b) illustration of the preparation of **Dns-non** and their application in electrical devices and bioscience.

Results and discussion

To construct a novel polysiloxane-based benzoxazine system, finding a proper condensation reaction that could bind the benzoxazine functional groups and the polysiloxane base together is of the primary concern. Yagci *et al.* reported the synthesis of polysiloxane containing benzoxazine moieties in the main chain using hydrosilylation reaction.[26] However, a Pt catalyst was applied and the residue of heavy metal catalysts may further limit the application of the products in biology or medical fields.[27] We fabricated polysiloxane-based benzoxazine (**P1**) *via* facile Mannich-type polycondensation with a high yield using bis[dimethyl(3-aminopropyl)silyl] ether (MM_2^{NH}) as the precursor (Scheme 1). An FT-IR spectra of the corresponding compounds provided evidence for the formation of the benzoxazine functionalized polymer **P1** (Fig. S1†). The structure of **P1** was further confirmed using ^{1}H NMR, ^{13}C NMR, and ^{29}Si NMR analysis (Fig. S2†). In addition, the molecular weight (M_n) of **P1** was about 7700 g mol^{-1}, and the PDI was about 1.21 (Table S1†). The increase of the molecular weight also indicates the success of the condensation polymerization. However, with the increase of the molecular weight of **P1**, the activity of the end group was reduced, which prevented the further growth of the main chain of **P1**. Mannich condensation is a flexible tool to incorporate a benzoxazine ring into polysiloxane-based materials.

Silicon-based films were prepared by an easy "casting" route [Scheme 1(b)]. The films were obtained and named **D1-non**, **D2-non**, and **D3-non**, respectively. Meanwhile, **C1-non**, **C2-non**, and **C3-non** were prepared without any use of rhodamine-B by the same method. Swelling analysis (Fig. S4†) showed that samples were cross-linked by physical cross-linking. Both hydrogen-bond interaction and π–π interaction between different polymer main chains resulted in cross-linking.[28] Contact angle measurement results (Fig. S5†) revealed that the surface energy of the films could be easily tuned by merely altering the molar ratio between MM_2^{NH} and BPA. SEM (Scanning Electron Microscopy) images (Fig. S6†) indicated that casting and the thermal treating approach that followed can produce **Dns-non** with homogenous surfaces.

As shown in Fig. 1(b), **Cns-non** emitted strong blue photoluminescence under 365 nm UV light. Fig. 1(a) illustrates the fluorescence from **C0-non**, **C1-non**, and **C2-non** excited at 365 nm. **Cns-non** emitted fluorescence in the spectral region of 460 nm under the excitation at 365 nm. According to the CIE diagram, the luminescence of **Cns-non** was blue, which was identical to the digital photograph in Fig. 1(b). Unlike carbon, a silicon atom has 5 empty 3d orbitals which can be used as electron acceptors. Luminescence was inferred to be generated by the lone pair electrons of N atoms coordinated with Si. The ligand field further split the 3d orbital of the Si atom, which was degenerated before coordination. Then, the electrons rearranged in the split orbitals resulting in a d–d transition, which could account for the luminescent properties of **Cns-non**.[29,30] **Dns-non** were transparent and presented strong red photoluminescence under natural light with the incorporation of rhodamine-B [Fig. 1(e) and (f)]. We directly stimulated the films using a wavelength of 520 nm. The emission spectra of **D1-non** were selected for further discussion. As shown in Fig. 1(d), the characteristic emission of rhodamine-B was found to be at a wavelength of 580 nm in **D1-non**. Based on CIE color

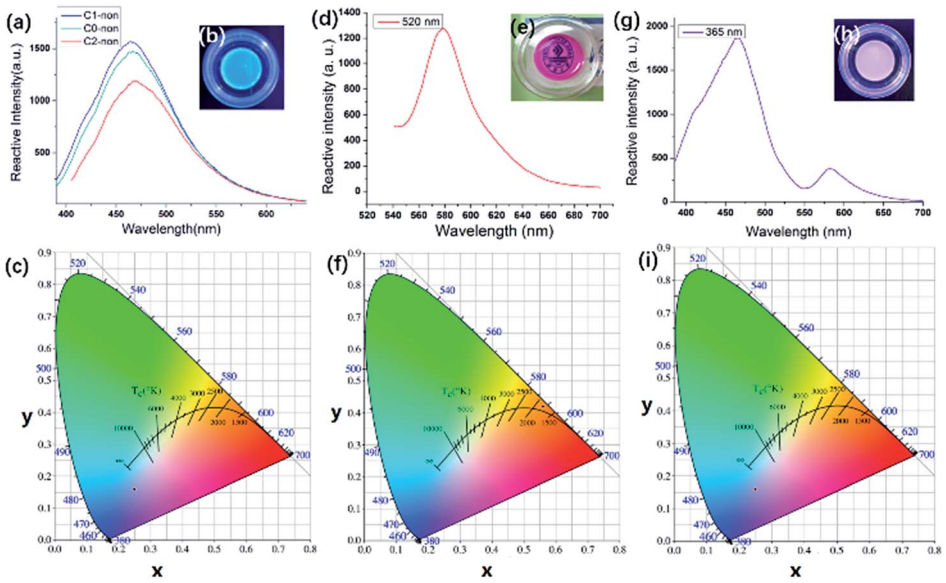

Fig. 1 (a) Solid-state photoluminescence spectra of **Cns-non** excited by a wavelength of 365 nm, (b) the photoluminescence image of **C1-non** excited by a wavelength of 365 nm, (c) the photograph of the CIE chromaticity diagrams for **Cns-non**, (d) the solid-state photoluminescence spectrum of **D1-non** excited by a wavelength of 520 nm, (e) the photoluminescence image of **D1-non** under natural light, (f) the photograph of the CIE chromaticity diagram for **D1-non** excited by a wavelength of 520 nm, (g) the solid-state photoluminescence spectrum of **D1-non** excited by a wavelength of 365 nm, (h) the photoluminescence image of **D1-non** excited by a wavelength of 365 nm, and (i) the photograph of the CIE chromaticity diagram for **D1-non** excited by a wavelength of 365 nm.

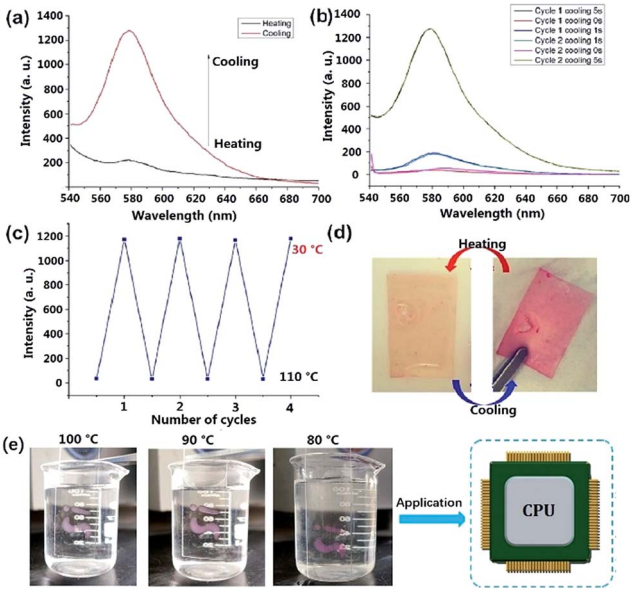

Fig. 2 (a) Solid-state photoluminescence spectra of **D1-non** excited by a wavelength of 520 nm measured after heating up and cooling down, respectively, (b) the change of fluorescence of **D1-non** excited by a wavelength of 520 nm with the time after cooling down, (c) PL intensity upon the cyclic switching of **D1-non** under alternating conditions of 110 and 30 °C, (d) digital image of **D1-non** (left: color faded after heating, right: color recovered after cooling down), and (e) digital photographs showing the possibility of using **Dns-non** as indicators for water temperature using **D0-non** as the demonstration.

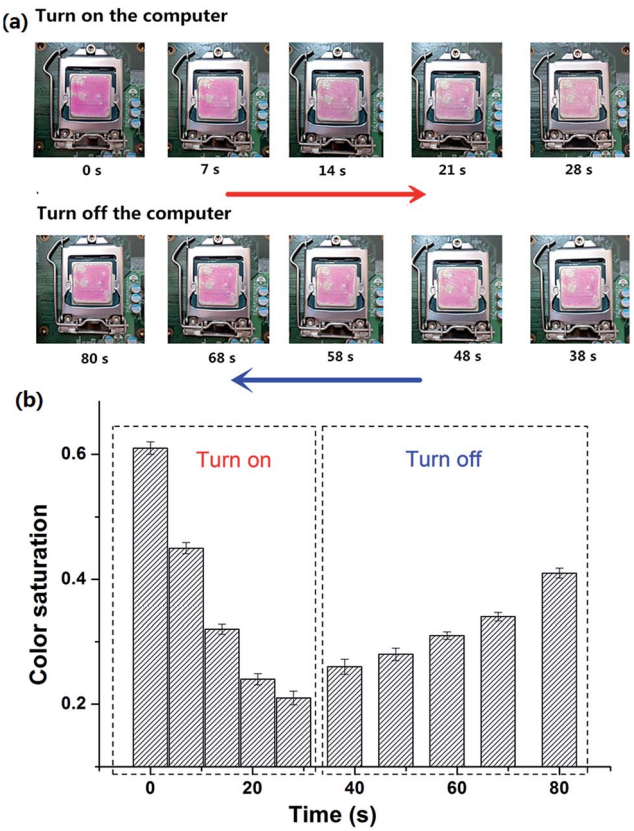

Fig. 3 (a) Digital images of a **D1-non** coated CPU with different running times illustrating the color changes, and (b) color saturation of the digital images of **D1-non** as a function of the computer running time. The error bars represent standard deviation (±S.D.).

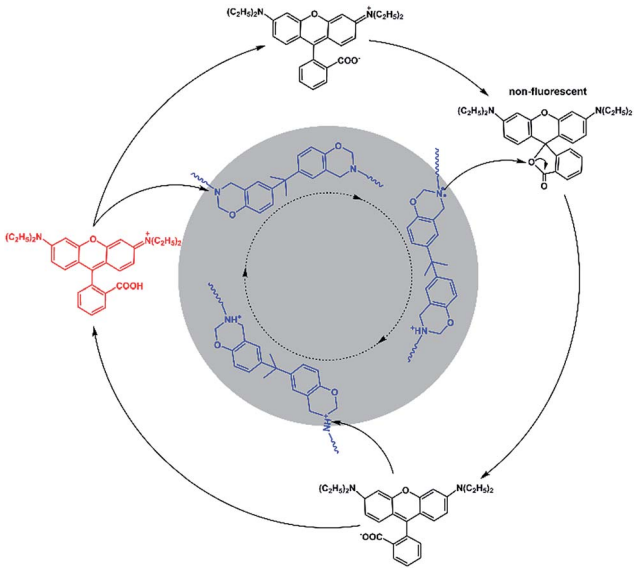

Fig. 4 Proposed reaction mechanism for the fluorescence of the **Dns-non** switch from "turn on" to "off "circulation.

coordinates calculated from the emission spectra, the bright red emission of **D1-non** could be observed by the naked eye when illuminated by natural light.

The surface color changed along with the variation of the temperature. We speculated that the UV absorption of **Dns-non** would change with temperature. The UV absorption of **D1-non** at different temperatures is shown in Fig. S10.† The absorption of **D1-non** was mainly derived from rhodamine-B. The absorption decreased with the increasing of the temperature, which fitted the fluorescence results. Rhodamine-B changed to its spirocyclic state at higher temperature and reduced the absorption. As a result, the fluorescence intensity decreased with the increasing of the temperature.

We focused on characterization of the dual color emissive property of **D1-non**, as dual color emissive materials may offer more potential for stimuli responsive properties. The characteristic peak of rhodamine-B could also be detected at approximately 580 nm, excited by a wavelength of 365 nm [Fig. 1(g)]. However, another emission peak was found at 460 nm, and the emission intensity at 460 nm was 3 times as big as the intensity at 580 nm. Identically, according to the CIE diagram, purple light (a combination of blue and red) could be observed when irradiated at 365 nm, which matched with the color observed by the naked eye. Interestingly, the emission colors of **D1-non** could be easily tuned from red (0.254, 0.172) to purple (0.592, 0.381) by just controlling the excitation wavelength. Excitation-dependent PL behavior can be useful in multi-color imaging applications.

Dns-non showed fascinating thermally responsive properties when undergoing a heating treatment. As illustrated in Fig. 2(d), after heating to 110 °C for 15 min, the red color of **D1-non** faded. However, **D1-non** regained its original color immediately when cooled to room temperature. Apparently, **Dns-non** presented thermally responsive behavior. Fluorescence spectra of **D1-non** at different temperatures were produced. As can be seen in Fig. 2(a), after thermal treatment at 110 °C for 15 min, the broad emission peak of **D1-non** at around 580 nm disappeared. However, remarkably, the cooling down of **D1-non** induced turn-on emission. Significant changes in emission intensity were observed as the temperature was varied [Fig. 2(b)]. It is obvious that the emission intensity reached the maximum value after cooling for 5 s, but it decreased dramatically at higher temperatures. Meanwhile, blue or red shift of emission peaks was not observed when the temperature was varied. To evaluate the reversibility of the switching operation upon variation of temperature, **D1-non** was then subjected to temperature cycling between 110 °C and 30 °C.

The fact that the luminescence switching operation could be repeated for four consecutive cycles without a fatigue phenomenon [Fig. 2(c)], indicated the fine reversibility of the two state switching process of photoluminescence. The cast films of **D0-non** to **D2-non** displayed similar responses to hot water. Taking **D0-non** as an example, as shown in Fig. 2(e), after heating at 100 °C in a hot water bath, the color of the transparent red film lightened, becoming close to colorless. However, when the temperature of the water dropped, the color was restored. This process could be repeated multiple times with good reproducibility. These results revealed the potential application of **Dns-non** films as temperature indicators. The pH stability was investigated using **D1-non** as an example. As shown in Fig. S12,† the fluorescence intensity of **D1-non** did not change significantly after being treated with solutions of varied pH. The physical cross-linking was efficient. In addition, the tertiary amine structure could act as a buffer, which could further reduce the effect of altering the pH. The results indicated that **Dns-non** exhibited good pH stability. The effect of common ions on **D1-non** were examined by treating **D1-non** with metal ions such as Cu^{2+}, Fe^{3+}, Mg^{2+}, Ba^{2+}, Zn^{2+}, Na^{+}, and K^{+} in 50% methanol solution at room temperature. The results are shown in Fig. S13.† The addition of Cu^{2+}, Al^{3+}, Mg^{2+}, Ba^{2+}, Na^{+}, Zn^{2+} and K^{+} ions led to no noticeable changes in the fluorescence intensity of **D1-non**, while Fe^{3+} caused apparent enhancement of the fluorescence intensity. The results indicated that Fe^{3+} caused rhodamine-B to change to its "ring-opening" state. The application environments of **Dns-non** do not contain common ions under normal conditions; therefore, the response to several common ions does not affect their applications.

High-performance CPUs built in to PCs have been developed to meet the requirement of higher PC performance. Thinner and more compact designs of CPU have lead to increased heat dissipation, making the CPU temperature rise and causing a shortened life, malfunction and failure of the CPU.[31,32] *In situ* indication of the surface temperature of the CPU visually should be taken seriously. Taking into account the temperature responsive property of **Dns-non**, we anticipated that their application could be expanded to *in situ* surface thermo-indication of the CPU. As depicted in Fig. 3(a), **D1-non** was coated onto the upper surface of the CPU. When the computer started running, the color of rhodamine-B faded. As the running time of the computer increased, the surface temperature of the

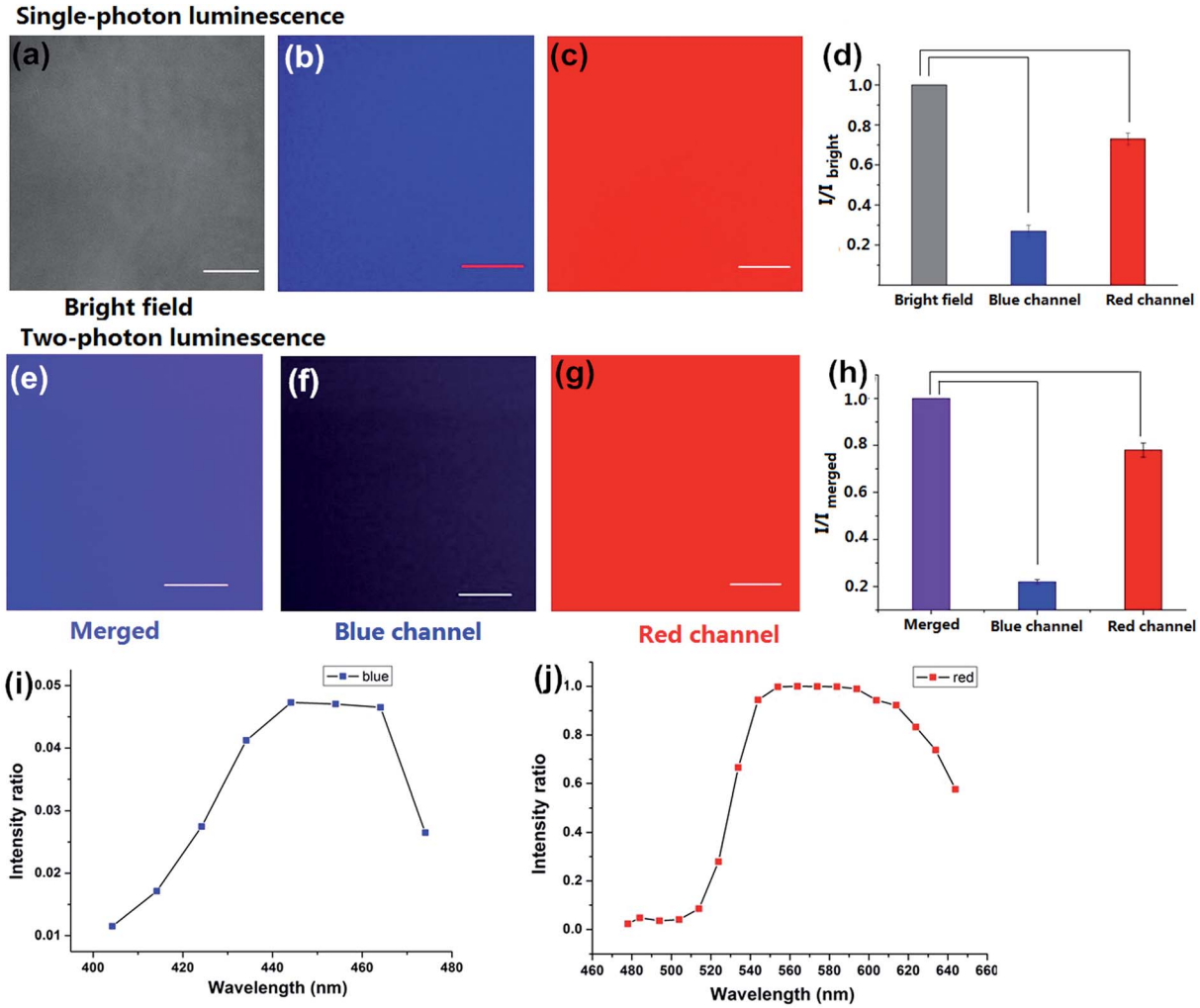

Fig. 5 Fluorescence images of **D1-non**: (a) bright field image, (b) image from the blue channel, (c) image from the red channel, and (d) quantified relative fluorescence intensities for (a)–(c). The error bars represent standard deviation (±S.D.). Two-photon fluorescence images of **D1-non**: (e) overlay of the blue and red channels, (f) image from the blue channel, (g) image from the red channel, and (h) quantified relative fluorescence intensities for (e)–(g). The error bars represent standard deviation (±S.D.). (i) Two-photon emission spectrum of **D1-non** in the blue region, and (j) two-photon emission spectrum of **D1-non** in the red region.

CPU raised gradually, and as a result, the fluorescence intensity of **D1-non** decreased. However, when the computer was closed, the fluorescence intensity of **D1-non** recovered as the surface temperature decreased. Furthermore, color saturation of these graphs was selected as a parameter to quantize the fluorescence change [Fig. 3(b)]. The change in color saturation was consistent with the color change observed by the naked eye. Monitoring the surface temperature of the CPU *in situ* was achieved by easily coating **D1-non** onto the CPU surface, which verified the potential application in electrical devices of **Dns-non**.

The control experiment (Fig. S8†) indicated that the fluorescence of rhodamine-B does not alter after a heating treatment, and the existence of common Si–O–Si chains does not affect the fluorescence of rhodamine-B. Furthermore, as illustrated in Scheme S1,† two kinds of tertiary amine, **M1** and **M2**, were selected as model compounds to get a deeper understanding of the mechanism. We could see from the inserted photograph in Fig. S9(b)† that the red color of Sample 1 faded at an evaluated temperature, and then recovered when cooled down. As shown in Fig. S9(a) and (b),† the fluorescence intensity of Sample 1 decreased after heating. As we expected, the fluorescence intensity increased when cooling down. As shown in Fig. S9(c) and (d),† Sample 2 exhibited a similar phenomenon to that of Sample 1. However, because of the existence of the –COOH group located in **M2**, the alkalinity of **M2** was weaker than that of **M1**. As a result, the decreasing proportion of the fluorescence intensity of Sample 2 is lower than that of Sample 1. A model control trial further confirmed the tertiary amine regulated reversible transition mechanism. In view of the two-state switching nature of rhodamine-B,[33,34] we deduced the mechanism of the fluorescent switch phenomenon of **Dns-non**. As illustrated in Fig. 4, the existence of a tertiary amine within **P1** led to the fluorescent switch behavior of **Dns-non**. Tertiary amines exert alkaline properties and have a tendency to react with acid to form a salt.[23–25] At room temperature, free rhodamine-B rested in its ring-open state. Meanwhile, **Dns-non**

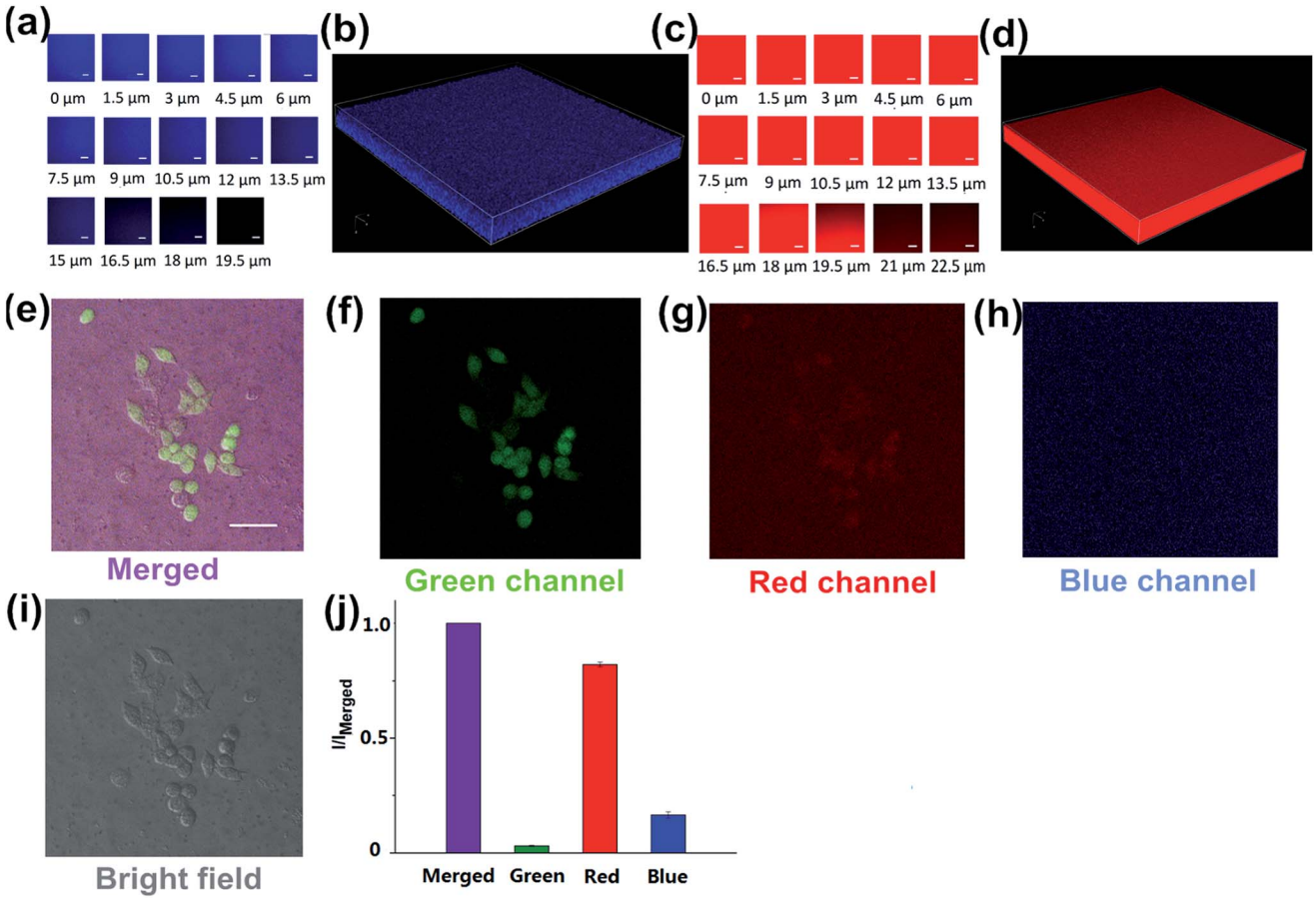

Fig. 6 (a) Planar images of **D2-non** in the blue channel. Magnification: 40×. (b) The 3D image of (a) at 0–19.5 μm depth. (c) Planar images of **D2-non** in the red channel. Magnification: 40×. (d) The 3D image of (c) at 0–19.5 μm depth, scale bar: 20 μm. Laser scanning confocal microscope photographs of HeLa cells spreading on **D2-non**. Magnification: 20×, scale bar: 50 μm: (e) overlay of the green, red, and blue channels, (f) from the green channel, (g) from the red channel, (h) from the blue channel, and (i) from the bright field. (j) Quantified relative fluorescence intensities for (e)–(h). The error bars represent standard deviation (±S.D.).

showed characteristic luminescence of rhodamine-B under the irradiation of natural light. When the temperature reached 110 °C, the tertiary amine group captured hydrogen in rhodamine-B at first. Then, the formed COO^- attacked the carbon atom adjacent to the benzene ring. As a result, rhodamine-B changed into its spirocyclic state. However, unlike most reported reactions between rhodamine-B and a primary amine without reversibility, the reaction between rhodamine-B and the tertiary amine presented good reversibility within a certain temperature range. When cooling down, N atoms in the polymer main chain attacked the spirocyclic ring, and formed an unstable intermediate. Thereafter, the fluorescence emerged along with the regeneration of rhodamine-B in its "open-cyclic" state. The "switch" process reached an equilibrium. Equilibrium shifted to the "close-cyclic" direction upon heating, whereas it moved to "open-cyclic" when the temperature dropped. This mechanism provided us with a new insight to build novel thermally responsive luminescent materials based on non-responsive groups, which further expands the application of thermally responsive materials.

To investigate the luminescence and the surface properties of **Dns-non**, fluorescence images of **D1-non** were captured using a Nikon A1MP confocal microscope. From the bright field image [Fig. 5(a)], phase separation was not found. The results indicated that the homogeneous phase of the film was obtained after rhodamine-B incorporation. **D1-non** exhibited strong and uniform blue luminescence when excited by a wavelength of 405 nm and captured by the blue channel [Fig. 5(b)]. Meanwhile, from the red channel, bright red luminescence could also be observed when excited by a wavelength of 561 nm [Fig. 5(c)]. The quantified relative fluorescence intensity for blue emission was weaker than for red emission [Fig. 5(d)]. These image results were consistent with the spectroscopic properties of **D1-non**.

Encouraged by the prominent results of the fluorescence images of **D1-non**, we decided to examine the fluorescence of **D1-non** using two-photon fluorescence microscopy. As depicted in Fig. 5(f) and (g), significant luminescence was observed when excited by a wavelength of 760 nm from both the blue channel and the red channel, which demonstrated that **D1-non** is a suitable material for showing superior two-photon fluorescence properties. Two-photon emission spectra of **D1-non** are depicted in Fig. 5(i) and (j), where two emission peaks were found at 450 nm and 580 nm, corresponding to blue and red

emissions, respectively. The intensity of the red emission derived from rhodamine-B was greater than the blue emission from the polymer, which was identical to the quantified relative fluorescence intensity result [Fig. 5(h)]. Results from the emission spectra further proved that two-photon fluorescence existed in **Dns-non**. The two-photon absorption cross-sections (δ) of the **D1-non** solution were determined using a two-photon-induced fluorescence method with the standard fluorescein in 1 mM NaOH aqueous solution as the reference. Fig. S11† shows the two-photon absorption cross-section spectra of **D1-non** in ethanol solution with a concentration of 10^{-5} mol L^{-1}. **D1-non** exhibited the highest cross-section of 232 GM when excited by a wavelength of 720 nm. The two-photon cross-sections of **D1-non** were higher than those of the reported pure rhodamine-B solutions. The enhanced cross-sections were deduced from the Fluorescence Resonance Energy Transfer (FRET) effect of **Pns**.

To our best knowledge, this represents the first report on thermally responsive materials that displayed unique two-photon fluorescence properties, which could expand the application of **Dns-non** into display or fluorescence imaging fields.

Since no 3D fluorescence imaging of silicon luminescent films has been reported previously, we were interested in exploiting the 3D luminescence image of **D2-non** in this regard. The 3D fluorescence images of **D2-non** were acquired using 405 and 561 nm excitation and fluorescence emission windows of 435–470 nm and 570–620 nm. As shown in Fig. 6(a) and (c), **D2-non** demonstrated homogenous strong fluorescence at a depth of up to 19.5 μm in both the blue channel and the red channel. The 3D imaging clearly confirmed the fine luminescence properties of **D2-non** [Fig. 6(b) and (d)]. Based on the measured uniform and stable surface properties, **Dns-non** were promising candidates for culturing cells on their upper surfaces. In addition, the unique fluorescence properties of **Dns-non** may enhance the image quality.

Polysiloxanes (**PDMS**) have received extensive attention in the materials and polymer fields because **PDMS** may offer many superior physical properties.[35–37] Bio-applications based on thermally responsive polysiloxane materials are also rare. Due to the importance of polysiloxane-based biomaterials for a range of applications, we investigated the application of **Dns-non** as cell adhesives. The toxicity of **Dns-non** towards living HeLa cells was assessed using the standard MTT assays. The MTT assays showed that **Dns-non** had little cytotoxicity to living cells (Fig. S14†). **D1-non** was used as the substrate to culture HeLa cells for inspecting the cytocompatibility of the material [Fig. S15†]. As shown in Fig. 6(e), the HeLa cells assembled into mature cytoskeletons, and the immunostaining results provided obvious evidence that the cell could bind to the **D1-non** substrate. These results made it clear that the physical cross-linking of **Dns-non** was complete. Films were very stable even when soaked in cell culture medium, showing that neither polymer nor rhodamine-B dissociated in cell culture medium. The cell assay indicated that the formation of adhesion is possible on silicone substrates. Hence **Dns-non** appeared as useful cell adhesives for the culture of cells on a surface. In addition, the quantified relative fluorescence intensities for the cell images [Fig. 6(j)] showed that both the intensity and contrast ratio of the image from the green channel was fairly weak. However, the merged image [Fig. 6(e)] showed improved contrast ratio and intensity due to the emission from the blue channel and the red channel derived from **D1-non** itself; thus, the fluorescence of **Dns-non** increased in external intensity when following cell imaging, thus enhancing the film quality.

Conclusions

In summary, new transparent films of **Dns-non** were fabricated based on **Pns** using rhodamine-B as a luminophore. Interestingly, **Dns-non** exhibited unique two-proton luminescence. Most importantly, the characteristic emission of rhodamine-B in **Dns-non** vanished after a heating treatment and recovered subsequently when cooling down. A proposed alkaline tuned reversible spirocyclization mechanism was put forward, which provided new perspective for the construction of thermally responsive materials based on conventional groups. Moreover, **Dns-non** expanded their application to devices when coated onto a CPU surface. Temperature changes of the CPU were easily detected by the naked eye *in situ via* by observing the color changes of **Dns-non**. Finally, the good cytocompatibility of **Dns-non** was demonstrated for HeLa cells which highlighted the potential of such thermally responsive materials for biological applications and cell culture. We expect that the design strategy described herein could be extended to construct more stimuli-responsive materials showing two-photon fluorescence and to explore their application in materials chemistry or bioscience.

Conflicts of interest

There are no conflicts to declare.

Acknowledgements

This work was financially supported by NSFC (21472067, 21672083), Taishan Scholar Foundation (TS201511041), and the startup fund of University of Jinan (309-10004, 1009428).

Notes and references

1 F. Ercole, T. P. Davis and R. A. Evans, *Nervenarzt*, 2010, **1**, 37–54.
2 Z. Song, K. Wang, C. Gao, S. Wang and W. Zhang, *Macromolecules*, 2016, **49**, 162–171.
3 S. Dong, Y. Luo, X. Yan, B. Zheng, X. Ding, Y. Yu, Z. Ma, Q. Zhao and F. Huang, *Angew. Chem.*, 2011, **123**, 1945–1949.
4 S. Uchiyama, Y. Matsumura, A. P. de Silva and K. Iwai, *Anal. Chem.*, 2003, **75**, 5926–5935.
5 Y. M. Lee and J. K. Shim, *Polymer*, 1997, **38**, 1227–1232.
6 Y.-C. Chen, R. Xie and L.-Y. Chu, *J. Membr. Sci.*, 2013, **442**, 206–215.
7 J. Feng, K. Tian, D. Hu, S. Wang, S. Li, Y. Zeng, Y. Li and G. Yang, *Angew. Chem.*, 2011, **50**, 8072–8076.
8 J. Zhou and H. Ma, *Chem. Sci.*, 2016, **7**, 6309–6315.

9 C. F. Chapman, Y. Liu, G. J. Sonek and B. J. Tromberg, *Photochem. Photobiol.*, 1995, **62**, 416–425.
10 R. E. Brewster, M. J. Kidd and M. D. Schuh, *Chem. Commun.*, 2001, **12**, 1134–1135.
11 M. Engeser, L. Fabbrizzi, M. Licchelli and D. Sacchi, *Chem. Commun.*, 1999, **18**, 1191–1192.
12 Y.-Q. Wang, Y.-Y. Zhang, F. Zhang and W.-Y. Li, *J. Mater. Chem.*, 2011, **21**, 6556–6562.
13 A. P. d. Silva, H. Q. N. Gunaratne, K. R. Jayasekera, S. O'Callaghan and K. R. A. S. Sandanayake, *Chem. Lett.*, 1995, **24**, 123–124.
14 Y. Al-Abed, T. H. Al-Tel, C. Schröder and W. Voelter, *Angew. Chem.*, 1994, **33**, 1499–1501.
15 H. Chen, H. Shang, Y. Liu, R. Guo and W. Lin, *Adv. Funct. Mater.*, 2016, **26**, 8128–8136.
16 D. Kim, H. Moon, S. H. Baik, S. Singha, Y. W. Jun, T. Wang, K. H. Kim, B. S. Park, J. Jung, I. Mook-Jung and K. H. Ahn, *J. Am. Chem. Soc.*, 2015, **137**, 6781–6789.
17 M. Pawlicki, H. A. Collins, R. G. Denning and H. L. Anderson, *Angew. Chem.*, 2009, **48**, 3244–3266.
18 Y. Gao, G. Feng, T. Jiang, C. Goh, L. Ng, B. Liu, B. Li, L. Yang, J. Hua and H. Tian, *Adv. Funct. Mater.*, 2015, **25**, 2857–2866.
19 C. S. Lim, G. Masanta, H. J. Kim, J. H. Han, H. M. Kim and B. R. Cho, *J. Am. Chem. Soc.*, 2011, **133**, 11132–11135.
20 B. Dong, X. Song, X. Kong, C. Wang, Y. Tang, Y. Liu and W. Lin, *Adv. Mater.*, 2016, **28**, 8755–8759.
21 M. Albota, D. Beljonne, J.-L. Brédas, J. E. Ehrlich, J.-Y. Fu, A. A. Heikal, S. E. Hess, T. Kogej, M. D. Levin, S. R. Marder, D. McCord-Maughon, J. W. Perry, H. Röckel, M. Rumi, G. Subramaniam, W. W. Webb, X.-L. Wu and C. Xu, *Science*, 1998, **281**, 1653–1656.
22 J. H. Lee, C. S. Lim, Y. S. Tian, J. H. Han and B. R. Cho, *J. Am. Chem. Soc.*, 2010, **132**, 1216–1217.
23 H. N. Kim, M. H. Lee, H. J. Kim, J. S. Kim and J. Yoon, *Chem. Soc. Rev.*, 2008, **37**, 1465–1472.
24 T. Nguyen and M. B. Francis, *Org. Lett.*, 2003, **5**, 3245–3248.
25 Z. Xu, L. Zhang, R. Guo, T. Xiang, C. Wu, Z. Zheng and F. Yang, *Sens. Actuators, B*, 2011, **156**, 546–552.
26 B. Aydogan, D. Sureka, B. Kiskan and Y. Yagci, *J. Polym. Sci., Part A: Polym. Chem.*, 2010, **48**, 5156–5162.
27 L. Xue, D. Wang, Z. Yang, Y. Liang, J. Zhang and S. Feng, *Eur. Polym. J.*, 2013, **49**, 1050–1056.
28 M. Arslan, B. Kiskan and Y. Yagci, *Macromolecules*, 2015, **48**, 1329–1334.
29 Y. Zuo, J. Cao and S. Feng, *Adv. Funct. Mater.*, 2015, **25**, 2754–2762.
30 Y. Zuo, Z. Gou, J. Cao, Z. Yang, H. Lu and S. Feng, *Chem.–Eur. J.*, 2015, **21**, 10972–10977.
31 K.-S. Kim, M.-H. Won, J.-W. Kim and B.-J. Back, *Appl. Therm. Eng.*, 2003, **23**, 1137–1144.
32 S. Gima, T. Nagata, X. Zhang and M. Fujii, *Heat Tran. Asian Res.*, 2005, **34**, 147–159.
33 X. Chen, S.-W. Nam, M. J. Jou, Y. Kim, S.-J. Kim, S. Park and J. Yoon, *Org. Lett.*, 2008, **10**, 5235–5238.
34 Q.-H. Liu, J. Liu, J.-C. Guo, X.-L. Yan, D.-H. Wang, L. Chen, F.-Y. Yan and L.-G. Chen, *J. Mater. Chem.*, 2009, **19**, 2018–2025.
35 F. Abbasi, H. Mirzadeh and A. A. Katbab, *Polym. Int.*, 2001, **50**, 1279–1287.
36 J. Chojnowski and M. Cypryk, in *Silicon-Containing Polymers*, Springer, 2000, pp. 3–41.
37 H. Yang, M. Xu, L.-X. Guo, H.-F. Ji, J.-Y. Wang, B.-P. Lin, X.-Q. Zhang and Y. Sun, *RSC Adv.*, 2015, **5**, 7304–7310.